

# Anomalous thermal expansion in a CuAl<sub>2</sub>-type superconductor CoZr<sub>2</sub>

Yoshikazu Mizuguchi<sup>1\*</sup>, Md. Riad Kasem<sup>1</sup>, Yoichi Ikeda<sup>2</sup>

<sup>1</sup>*Department of Physics, Tokyo Metropolitan University, Hachioji, Tokyo 192-0397, Japan.*

<sup>2</sup>*Institute for Materials Research, Tohoku University, Sendai, Miyagi 987-6543, Japan*

E-mail: mizugu@tmu.ac.jp

Keywords: negative thermal expansion, zero thermal expansion, superconductor, CoZr<sub>2</sub>, neutron diffraction

In this work, we show that the CuAl<sub>2</sub>-type superconductor CoZr<sub>2</sub> and alloyed systems exhibit anomalous thermal expansion in a wide temperature range. We performed neutron powder diffraction and X-ray powder diffraction on CoZr<sub>2</sub> and observed remarkably anisotropic thermal expansion with a *c*-axis negative thermal expansion constant of  $\alpha_c < -15 \mu\text{K}^{-1}$  in a wide temperature range of  $T = 50\text{--}573$  K. With decreasing temperature, the lattice constant *a* decreases, while the lattice constant *c* continuously increases in CoZr<sub>2</sub>. The origin of the anisotropic shrinkage/expansion of the *a*-axis/*c*-axis by cooling is explained by the small change in the Co-Zr bond and the systematic decrease in the Zr-Co-Zr angle. Similar thermal expansion was observed in alloyed systems, (Fe,Co,Ni)Zr<sub>2</sub> and (Fe,Co,Ni,Rh,Ir)Zr<sub>2</sub>, which suggests that the phenomenon is common feature in the *Tr*Zr<sub>2</sub> system. We propose that zero-thermal expansion metals would be achieved by optimizing the contrasting thermal expansion of *a*-axis and *c*-axis in *Tr*Zr<sub>2</sub>.

## 1. Introduction

Materials that exhibit negative thermal expansion (NTE) or zero thermal expansion (ZTE) have been developed in a wide range of materials because that can be used for various applications including the use in precision instruments.<sup>[1-5]</sup> The typical NTE material is ZrW<sub>2</sub>O<sub>8</sub>, which exhibits a large isotropic NTE over a wide range of temperatures (*T*).<sup>[4]</sup> In ZrW<sub>2</sub>O<sub>8</sub>, the origin of the NTE is its characteristic flexible network on the atomic bonding and linkage of the units. In addition, NTE has been observed in various compounds that exhibit a phase transition. The driving force includes a metal-insulator transition,<sup>[5,6]</sup>

magnetovolume effects,<sup>[7,8]</sup> intermetallic charge transfer,<sup>[9,10]</sup> valence crossover (or transition),<sup>[11,12]</sup> and ferroelectric transition.<sup>[13,14]</sup> Furthermore, NTE has been observed in various superconductors or related antiferromagnetic phases.<sup>[15-21]</sup> In most cases of NTE in superconductors, the origin of the NTE is linked to the emergence of the superconducting order parameter; hence, the NTE is typically observed below the transition temperature ( $T_c$ ).<sup>[3]</sup> In addition, there are superconductors that exhibit NTE at temperatures well above its  $T_c$ : the typical example is the BSCCO superconductor.<sup>[17]</sup> Since the thermal expansion characteristics of superconductors is critical when fabricating superconducting wires or films, studies on thermal expansion on superconductors have been performed in a wide temperature range so far.<sup>[22-24]</sup>

Here, we show anomalously anisotropic thermal expansion in  $\text{CoZr}_2$  and alloyed  $\text{TrZr}_2$  (Tr: Fe, Co, Ni, Rh, Ir). We observed contrasting thermal expansions of the  $a$ -axis and the  $c$ -axis in the tetragonal unit cell. In the wide temperature range of  $T = 50\text{--}572$  K ( $T = 572$  K is the highest temperature examined in this study),  $\text{CoZr}_2$  exhibits continuous positive thermal expansion (PTE) of the  $a$ -axis and NTE of the  $c$ -axis. As a result of the contrasting expansions, the lattice volume does not remarkably decrease by the decrease in temperature.

**Figure 1** shows the schematic images of the crystal structure of  $\text{CoZr}_2$  with a  $\text{CuAl}_2$ -type tetragonal structure (space group #140). The framework is composed of the  $\text{CoZr}_8$  polyhedron units, which are stacked along the  $c$ -axis.  $T_c$  of  $\text{TrZr}_2$  with  $\text{Tr} = \text{Ni, Co, Rh, Ir}$  is 3.2, 5.2, 11.3, and 7.5 K, respectively.<sup>[25]</sup> The electronic density of states (DOS) near the Fermi energy ( $E_F$ ) is mainly composed of the hybridization of Zr- $d$  and Co- $d$  orbitals.<sup>[26]</sup> Noticeably, the  $T_c$  of  $\text{CoZr}_2$  increases with application of external pressures:  $T_c = 9.5$  K at 8 GPa.<sup>[26]</sup> The huge pressure effect implies the flexible crystal structure, which would largely modify the electronic DOS and/or electron-phonon coupling in the system under high pressures. In addition, we recently developed alloyed compounds of  $\text{TrZr}_2$  by drawing the high-entropy-alloy (HEA) concept.<sup>[27-29]</sup> Interestingly, the  $T_c$  of  $\text{TrZr}_2$  increases with increasing lattice constant  $c$ , while the variation of the element, the concentration, configurational entropy of mixing at the  $\text{Tr}$  site do not have an impact on  $T_c$  though the strong disorder was introduced by alloying on the  $\text{Tr}$  site. This trend also implies the importance of chemical bonds along the  $c$ -axis in the  $\text{TrZr}_2$  superconductors. Motivated by those backgrounds on the relationship between superconductivity and the crystal structure in  $\text{TrZr}_2$ , we decided to perform crystal structure analyses for  $\text{CoZr}_2$  and the alloyed compounds in a wide temperature range.

## 2. Results and discussion

**Figure 2(a)** shows the NPD patterns for  $\text{CoZr}_2$  taken at  $T = 7, 50, 100, 170$ , and  $293$  K (room temperature). The profiles at  $T = 7$  and  $293$  K are similar, and no crystal structural transition and magnetic ordering were observed. As displayed in Fig. 2(b), we observed a decrease in the lattice constant  $a$  (from the 200 peak) and an increase in the lattice constant  $c$  (from the 002 peak). To obtain the temperature dependences of lattice constants, the NPD patterns were analyzed by Rietveld method with a three-phase mode as shown in Fig. 2(c) and Fig. S2 (supporting information); the refined structural parameters are summarized in Table I. Here, we identified the two impurity phases of  $\text{CoZr}_3$  (16%, space group #63) and  $\text{CoZr}$  (5%, space group #225). Figures 2(d–f) show the temperature dependences of lattice constants  $a$ ,  $c$ , and  $V$  for  $\text{CoZr}_2$ . With decreasing temperature, the lattice constant  $a$  decreases, which is PTE, and the lattice constant  $c$  increases, which is NTE. The high-temperature XRD results also exhibit the same trend (see supporting information for the XRD patterns). Since the  $a$ -axis and the  $c$ -axis exhibit contrasting PTE/NTE, the lattice volume ( $V$ ) does not show monotonous changes. The results imply that the  $\text{TrZr}_2$  system is potential ZTE material after tuning the PTE and NTE of the  $a$ - and  $c$ -axis. For the NTE of the  $c$ -axis, the thermal expansion constant ( $\alpha_c$ ) was estimated as  $-15 \mu\text{K}^{-1}$  for low-temperature NPD data and  $-28 \mu\text{K}^{-1}$  for high-temperature XRD data using a formula of  $\alpha_c = [1/c(300 \text{ K})]/(dc/dT)$ . The reported value of the linear thermal expansion constant ( $\alpha$ ) for typical NTE materials are  $\alpha = -9 \mu\text{K}^{-1}$  for  $\text{ZrW}_2\text{O}_8$ ,<sup>[4]</sup>  $-26 \mu\text{K}^{-1}$  for  $\text{LaFe}_{10.5}\text{Co}_{1.0}\text{Si}_{1.5}$ ,<sup>[7]</sup>  $-0.7 \mu\text{K}^{-1}$  for  $\text{Ba}(\text{Fe}_{0.962}\text{Co}_{0.038})_2\text{As}_2$ ,<sup>[15]</sup>  $-0.8 \mu\text{K}^{-1}$  for  $\text{PrFeAsO}$ ,<sup>[30]</sup> and  $-87 \mu\text{K}^{-1}$  for  $\text{BSCCO}$ .<sup>[17]</sup> We noticed that the  $\alpha_c$  observed in  $\text{CoZr}_2$  is comparable to that of  $\text{LaFe}_{10.5}\text{Co}_{1.0}\text{Si}_{1.5}$  and relatively large among NTE of superconductors. The linear thermal expansion constant along the  $a$ -axis ( $\alpha_a$ ) was also estimated and shown in Fig. 2(a).

To understand the origin of the anomalous (or anisotropic) thermal expansion of the  $a$ -axis and the  $c$ -axis, the atomic distances of Co-Zr, Co-Co, and Zr-Zr are evaluated from NPD and XRD data and summarized in Table I (See Fig. 1 for the labels of the distances and the angle). The Co-Co (i) distance is directly linked to the lattice constant  $c$ , and it increases with decreasing temperature. The Co-Co (ii) and Zr-Zr (ii) distances decrease with decreasing temperature, which can be understood with the  $a$ -axis compression. We found that the Co-Zr and Zr-Zr (i) distances do not largely change at low temperatures. Since the Zr-Zr (i) distance is relatively larger than that of the other bonds, and the Co-Zr bond should be essential for this compound, we consider that the origin of the  $c$ -axis expansion is linked to the bonding character of the Co-Zr bond. As a fact, Zr-Co-Zr angle shows systematic

decrease with decreasing temperature. Therefore, we conclude that the anomalous anisotropic thermal expansion (elongation of the unit cell) in  $\text{CoZr}_2$  is induced by the robust Co-Zr distance to the temperature change and the flexible Zr-Co-Zr angle in the  $\text{CoZr}_8$  polyhedron. As reviewed in Ref. [31], NTE in  $\text{ReO}_3$ -type materials is caused by flexibility of structure, and the origin of the flexible bonds was discussed in terms of anisotropic atomic vibration (displacement). To examine the presence of anisotropic atomic displacement parameters in  $\text{CoZr}_2$ , we performed anisotropic analyses of atomic displacement parameters,  $U_{11}$  and  $U_{33}$  along  $a$ -axis and  $c$ -axis, respectively. Since anisotropic analysis for the Co site was not successful at low temperatures, only the results for  $T = 293$  K are shown. The estimated values are  $U_{11}(\text{Co}) = 0.052(6) \text{ \AA}^2$ ,  $U_{33}(\text{Co}) = 0.013(6) \text{ \AA}^2$ ,  $U_{11}(\text{Zr}) = 0.023(2) \text{ \AA}^2$ , and  $U_{33}(\text{Zr}) = 0.014(2) \text{ \AA}^2$ . **Figure 3** displays a schematic image of crystal structure of  $\text{CoZr}_2$  with displacement ellipsoids represented by 90% probability of the displacement parameters. The  $U_{11}(\text{Co})$  is clearly larger than other parameters. This would be caused by anisotropic Co vibrations and/or displacements. To understand the origin, local structure analyses are needed; extended X-ray absorption fine structure (EXAFS) or pair density function (PDF) analyses will give further information on the origin of NTE in  $\text{CoZr}_2$ . Similar contrasting axes thermal expansion has also been observed in Cordierite ( $\text{Mg}_2\text{Al}_4\text{Si}_5\text{O}_{18}$ ), and that was well explained by ab-initio molecular dynamics (MD) simulation.<sup>[32]</sup> Therefore, MD simulation should be useful to understand the origin of NTE in the  $c$ -axis of  $\text{CoZr}_2$ .

In this study, we examined low-temperature crystal structures for the alloyed compounds,  $(\text{Fe},\text{Co},\text{Ni})\text{Zr}_2$  and  $(\text{Fe},\text{Co},\text{Ni},\text{Rh},\text{Ir})\text{Zr}_2$  as well. For  $(\text{Fe},\text{Co},\text{Ni})\text{Zr}_2$ , three-phase analysis same as the case of  $\text{CoZr}_2$  was performed. For,  $(\text{Fe},\text{Co},\text{Ni},\text{Rh},\text{Ir})\text{Zr}_2$ , due to the presence of unknown impurity peaks, we performed single-phase analysis. See supporting information for the Rietveld refinement results for those samples. Furthermore, high-temperature XRD was performed to roughly estimate lattice constants at high temperatures using samples taken from different batches (see Fig. S5 in supporting information). In **Figs. 4(a–f)**, the temperature dependences of lattice constants  $a$ ,  $c$ , and  $V$  for those alloyed samples are shown. Noticeably, the contrasting thermal expansion, PTE of the  $a$ -axis and NTE of the  $c$ -axis, was observed for both  $(\text{Fe},\text{Co},\text{Ni})\text{Zr}_2$  and  $(\text{Fe},\text{Co},\text{Ni},\text{Rh},\text{Ir})\text{Zr}_2$ . In addition, the trend on the temperature evolution of the  $\text{TrZr}_8$  polyhedron is similar; namely, the change in  $\text{Tr-Zr}$  distance is small and the  $\text{Zr-Tr-Zr}$  angle systematically decreases with decreasing temperature (see Tables in supporting information for the refined parameters).

We briefly discuss about the origin of the anomalous (contrasting anisotropic) thermal expansion in  $\text{TrZr}_2$ . According to the binary Co-Zr phase diagram, the  $\text{CuAl}_2$ -type

CoZr<sub>2</sub> phase is congruent melting, and no structural transition is expected at temperatures higher than 572 K. In addition, no magnetic ordering was observed in our NPD results. Furthermore, the NTE of the *c*-axis occurs at temperatures well above  $T_c$  of 6.0 K in CoZr<sub>2</sub>. Although we have to confirm the possibility of the change in valence state of *Tr* (i.e. electronic and bonding states of *Tr*) to exclude the possibility of valence-state-driven NTE, we here propose that the robust *Tr*-Zr bonds and the flexibility of the bond angle in the *Tr*Zr<sub>8</sub> polyhedron is the origin of the anomalous anisotropic thermal expansion in *Tr*Zr<sub>2</sub>.

Here, we discuss prospects on the observed anomalous thermal expansion in *Tr*Zr<sub>2</sub>. Since the *a*-axis and the *c*-axis of *Tr*Zr<sub>2</sub> show contrasting thermal expansion (PTE and NTE), one of the expected applications is ZTE by tuning the changes in both axes. As a fact, the examined samples exhibit small expansion of the volume by cooling. The volume compression rate calculated by  $[V(293\text{ K})-V(50\text{ K})]/V(293\text{ K})$  for CoZr<sub>2</sub>, (Fe,Co,Ni)Zr<sub>2</sub>, and (Fe,Co,Ni,Rh,Ir)Zr<sub>2</sub> is -0.55%, -0.46%, and -0.11%, respectively; here we used the data at 50 K because the NTE of the *c*-axis was observed down to 50 K for CoZr<sub>2</sub>. The trend suggests that alloying the *Tr* site by the HEA concept would be useful for achieving ZTE in *Tr*Zr<sub>2</sub>. Furthermore, tunable volume thermal expansion is also a manufacturing advantage in the field of superconductivity application.<sup>[22–24]</sup> Comparing the estimated linear thermal expansion constants,  $\alpha_a$  and  $\alpha_c$ , we noticed that the *a*-axis thermal expansion below room temperature is affected and suppressed by alloying (with increasing configurational entropy of mixing at the *Tr* site), while the *c*-axis thermal expansion is not affected by alloying. It is known that chemical substitution introduces local disorder in materials and modify thermal expansion.<sup>[31]</sup> Therefore, tuning of the configurational entropy of mixing would be useful to achieve zero-thermal expansion. Although we have not revealed the origin of the suppression of the *a*-axis thermal expansion, the large isotropic displacement parameter ( $U_{iso}$ ) for the Zr site for the alloyed systems, which are shown in **Fig. 5**, should be linked to the weakened *a*-axis thermal expansion by alloying.

Another future prospect is the enhancement of  $T_c$  in *Tr*Zr<sub>2</sub>. As discussed in Ref. 29, a larger lattice constant *c* is preferable for a higher  $T_c$  in *Tr*Zr<sub>2</sub>. Therefore, if we could clarify the origin of the NTE of the *c*-axis in *Tr*Zr<sub>2</sub>, a new superconductor with a  $T_c$  exceeding 12 K, which is higher than the  $T_c$  of RhZr<sub>2</sub>, would be designed. In addition, the crystal structure analyses under high pressure are desired to clarify the origin of the enhancement of  $T_c$  by pressure and the link to the anomalous thermal expansion in *Tr*Zr<sub>2</sub> reported here.

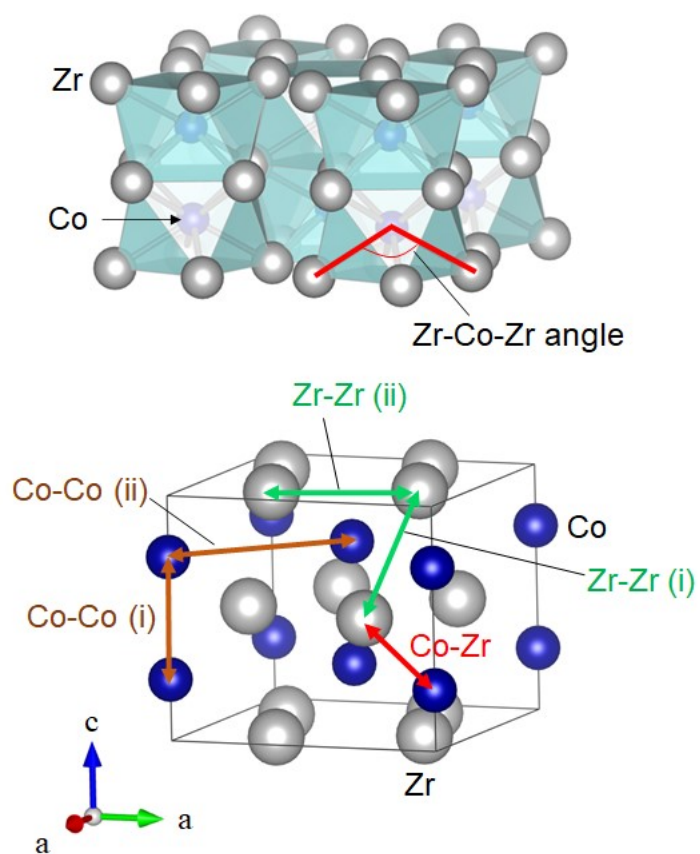


**Fig.1.** Schematic images of the crystal structure of  $\text{CoZr}_2$ . The solid line in the lower figure shows the unit cell of  $\text{CoZr}_2$ .

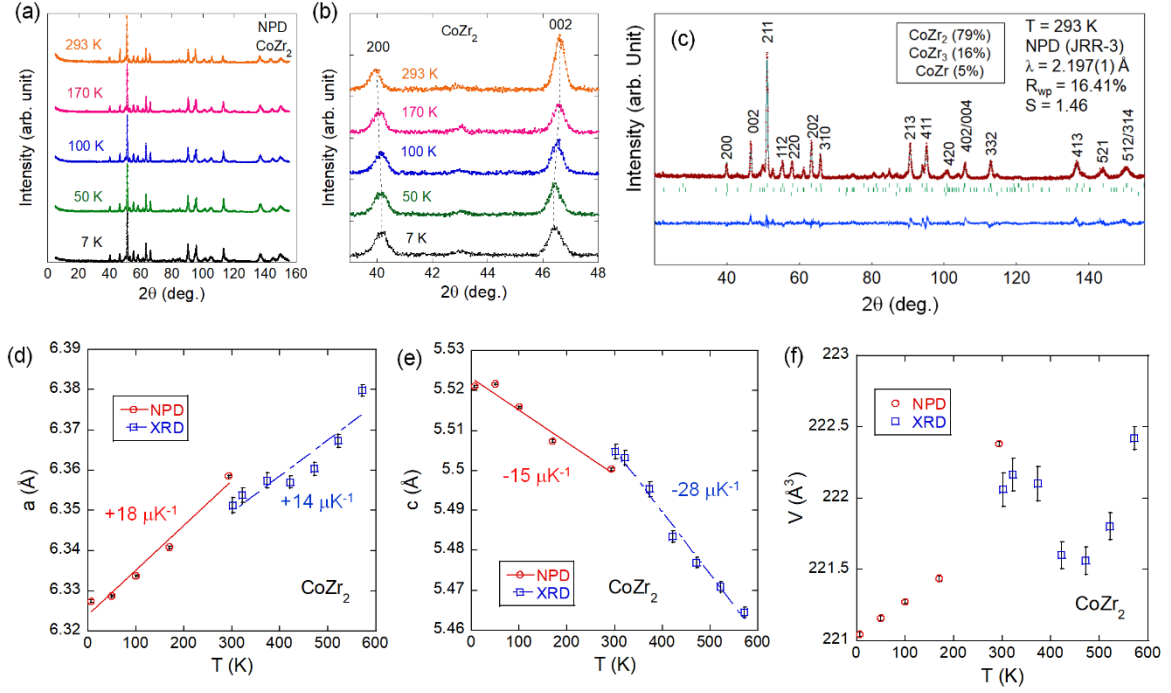


**Fig. 2.** (a) NPD patterns for CoZr<sub>2</sub> collected at  $T = 7, 50, 100, 170, 293$  K. (b) NPD patterns near the 200 and 002 peaks. (c) Rietveld refinement results for the NPD data for CoZr<sub>2</sub> ( $T = 293$  K). The numbers indicate Miller indices. (d–f) Temperature dependence of lattice constant  $a$ ,  $c$ , and  $V$  for CoZr<sub>2</sub>. NPD and XRD denote neutron powder diffraction and X-ray powder diffraction, respectively. The error bars in (d,e,f) are a standard error determined by Rietveld refinement. The estimated linear thermal expansion constants are  $+18 \pm 2 \mu\text{K}^{-1}$  ( $a$  by low-temperature NPD),  $+14 \pm 3 \mu\text{K}^{-1}$  ( $a$  by high-temperature XRD),  $-15 \pm 2 \mu\text{K}^{-1}$  ( $c$  by low-temperature NPD), and  $-28 \pm 1 \mu\text{K}^{-1}$  ( $c$  by high-temperature XRD).

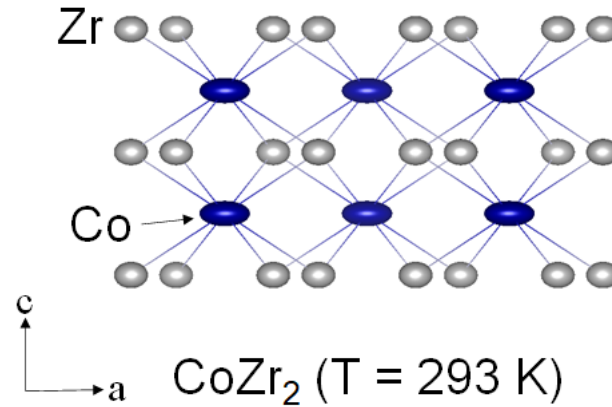


**Fig. 3.** Schematic image of crystal structure of CoZr<sub>2</sub> ( $T = 293$  K) drawn with 90% probability of anisotropic atomic displacement parameters  $U_{11}$  and  $U_{33}$ .

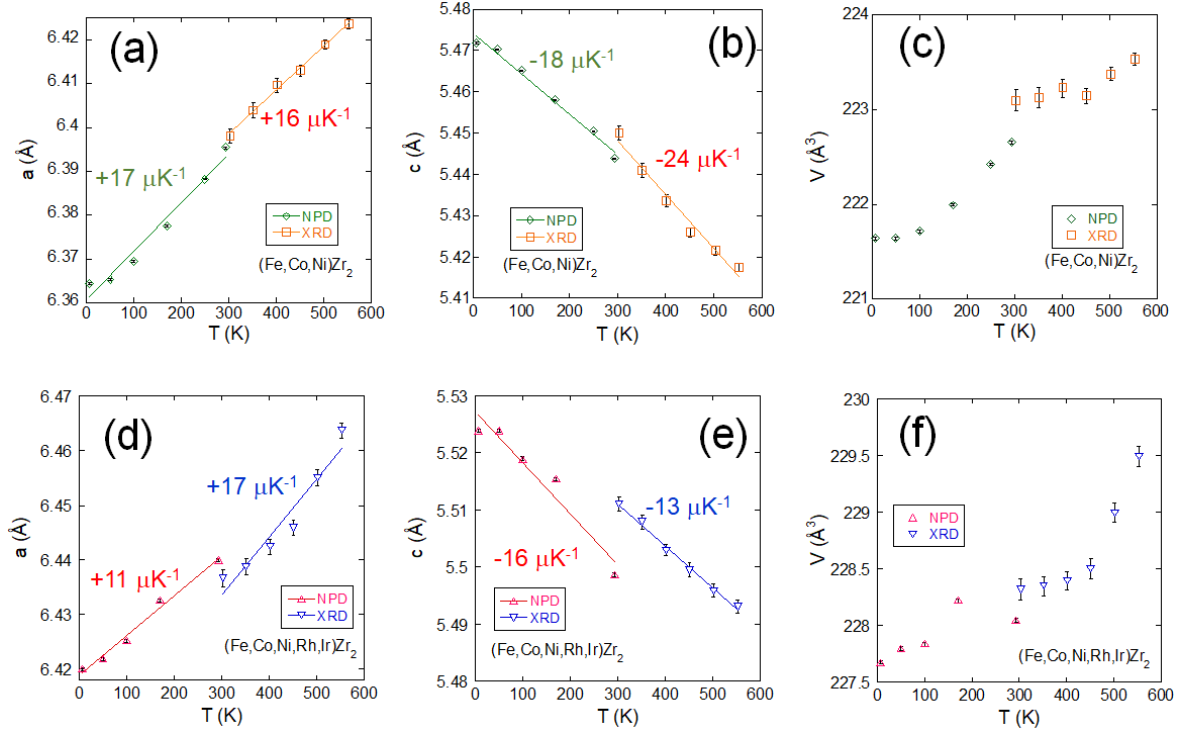


**Fig. 4.** Lattice constants determined from NPD and XRD for alloyed  $Tr\text{Zr}_2$ . The error bars are a standard error determined by Rietveld refinement. (a–c) Temperature dependence of lattice constant  $a$ ,  $c$ , and  $V$  for  $\text{Fe}_{1/3}\text{Co}_{1/3}\text{Ni}_{1/3}\text{Zr}_2$ . The estimated linear thermal expansion constants are  $+17 \pm 2 \mu\text{K}^{-1}$  ( $a$  by low-temperature NPD),  $+16 \pm 1 \mu\text{K}^{-1}$  ( $a$  by high-temperature XRD),  $-18 \pm 1 \mu\text{K}^{-1}$  ( $c$  by low-temperature NPD), and  $-24 \pm 2 \mu\text{K}^{-1}$  ( $c$  by high-temperature XRD). (d–f) Temperature dependence of lattice constant  $a$ ,  $c$ , and  $V$  for  $\text{Fe}_{0.2}\text{Co}_{0.2}\text{Ni}_{0.2}\text{Rh}_{0.2}\text{Ir}_{0.2}\text{Zr}_2$ . The estimated linear thermal expansion constants are  $+11 \pm 1 \mu\text{K}^{-1}$  ( $a$  by low-temperature NPD),  $+17 \pm 2 \mu\text{K}^{-1}$  ( $a$  by high-temperature XRD),  $-16 \pm 2 \mu\text{K}^{-1}$  ( $c$  by low-temperature NPD), and  $-13 \pm 1 \mu\text{K}^{-1}$  ( $c$  by high-temperature XRD).



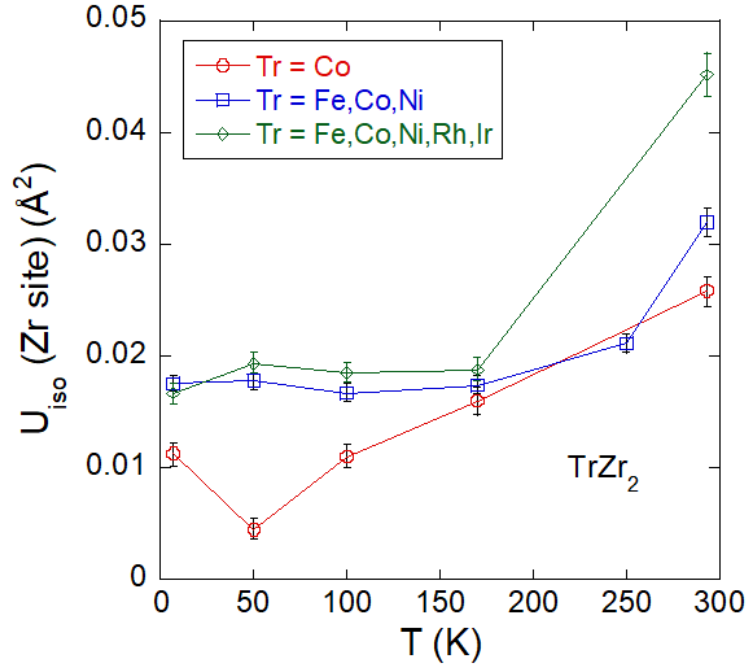


**Fig. 5.** Temperature dependences of isotropic displacement parameter ( $U_{\text{iso}}$ ) for  $\text{CoZr}_2$ ,  $(\text{Fe,Co,Ni})\text{Zr}_2$ , and  $(\text{Fe,Co,Ni,Rh,Ir})\text{Zr}_2$ .

**Table I.** Structural parameters of  $\text{CoZr}_2$  obtained from the Rietveld refinement. The atomic coordinates for the Zr and Co site are  $(x, x+0.5, 0)$  and  $(0, 0, 0.25)$ , respectively.

	$T = 293 \text{ K}$	$T = 170 \text{ K}$	$T = 100 \text{ K}$	$T = 50 \text{ K}$	$T = 7 \text{ K}$
Space group	$I4/mcm$ (#140)				
$a$ ( $\text{\AA}$ )	6.3584(3)	6.3409(3)	6.3337(3)	6.3287(3)	6.3274(3)
$c$ ( $\text{\AA}$ )	5.5002(3)	5.5074(3)	5.5159(2)	5.5217(2)	5.5211(3)
$V$ ( $\text{\AA}^3$ )	222.37(2)	221.44(2)	221.28(2)	221.16(2)	221.04(2)
$R_{\text{wp}}$ (%)	16.41	16.02	14.31	13.84	14.8
$S$	1.46	1.64	1.54	1.50	1.87
$x$ (Zr)	0.1710(2)	0.1720(2)	0.1717(2)	0.1715(2)	0.1721(2)
$U_{\text{iso}}$ (Co) ( $\text{\AA}^2$ )	0.034(3)	0.07(2)	0.08(2)	fixed	fixed
$U_{\text{iso}}$ (Zr) ( $\text{\AA}^2$ )	0.0258(13)	0.0160(13)	0.0110(10)	0.0045(9)	0.0112(11)
Co-Zr distance ( $\text{\AA}$ )	2.7293(12)	2.7223(12)	2.7218(11)	2.7214(11)	2.7195(11)
Co-Co (i) distance ( $\text{\AA}$ )	2.7501(2)	2.7537(2)	2.75795(11)	2.76085(11)	2.7606(2)
Co-Co (ii) distance ( $\text{\AA}$ )	4.4961(3)	4.4837(3)	4.4786(3)	4.4751(3)	4.4742(2)
Zr-Zr (i) distance ( $\text{\AA}$ )	3.0954(12)	3.0887(12)	3.0942(12)	3.0979(12)	3.0926(9)
Zr-Zr (ii) distance ( $\text{\AA}$ )	3.334(2)	3.321(2)	3.319(2)	3.317(2)	3.314(2)
Zr-Co-Zr angle (deg.)	119.49(3)	119.24(3)	119.12(3)	119.04(3)	119.00(4)

### 3. Conclusion

We have analyzed the crystal structure of the  $\text{CuAl}_2$ -type transition-metal zirconides  $\text{CoZr}_2$ ,  $(\text{Fe},\text{Co},\text{Ni})\text{Zr}_2$ , and  $(\text{Fe},\text{Co},\text{Ni},\text{Rh},\text{Ir})\text{Zr}_2$  using neutron powder diffraction at low temperatures and X-ray powder diffraction at high temperatures. With decreasing temperature, all samples showed  $a$ -axis shrinkage (PTE) and  $c$ -axis expansion (NTE). The anomalous (contrasting and anisotropic) thermal expansion of the  $a$ -axis and the  $c$ -axis in  $\text{TrZr}_2$  is explained by the small change in the  $\text{Tr-Zr}$  distance and the systematic decrease in the  $\text{Zr-Tr-Zr}$  angle, which results in elongation of the unit cell along the  $c$ -axis. Although the origin of the structural change is still unclear, we consider that the flexible bonding of the  $\text{TrZr}_8$  polyhedron units is essential for the NTE of the  $c$ -axis in  $\text{TrZr}_2$ .

### 4. Experimental Section

#### 4-1. Sample Preparation

The polycrystalline samples of  $\text{CoZr}_2$ ,  $\text{Fe}_{1/3}\text{Co}_{1/3}\text{Ni}_{1/3}\text{Zr}_2$  (abbreviated as  $(\text{Fe},\text{Co},\text{Ni})\text{Zr}_2$ ), and  $\text{Fe}_{0.2}\text{Co}_{0.2}\text{Ni}_{0.2}\text{Rh}_{0.2}\text{Ir}_{0.2}\text{Zr}_2$  (abbreviated as  $(\text{Fe},\text{Co},\text{Ni},\text{Rh},\text{Ir})\text{Zr}_2$ ) were prepared by arc melting using powders of Fe (99.9%), Co (99%), Ni (99.9%), Rh (99.9%) and Ir (99.9%) and plates of Zr (99.2%) as described in Ref. 29.

#### 4-2. Characterization

The phase purity and the crystal structure were examined by X-ray powder diffraction (XRD) with  $\text{Cu-K}\alpha$  radiation by the  $\theta$ - $2\theta$  method on Miniflex-600 (RIGAKU) equipped with a high-resolution semiconductor detector D/tex-Ultra. For high-temperature XRD on Miniflex-600, the sample temperature was controlled by the BTS500 attachment. For low-temperature experiments, we performed neutron powder diffraction (NPD) with a HERMES diffractometer<sup>[33]</sup> installed at the T1-3 guide port in the JRR-3 of the Japan Atomic Energy Agency, Tokai. A thermal neutron beam was monochromatized to be  $2.197(1)$  Å with a vertically-focused Ge (331) monochromator. Typical instrumental parameters were determined by analyzing line positions and line shapes of a standard reference material ( $\text{LaB}_6$ , NIST660c).<sup>[34]</sup> Powder samples were sealed in a vanadium cylinder cell with  $\phi 6$  mm-diameter (thickness 0.1 mm) and  $\sim 60$ mm-length in a  $^4\text{He}$  gas atmosphere. A closed-cycle refrigerator was used to cool the samples and controlled from a base temperature ( $T \sim 7$  K) to room temperature. Note that the samples used in NPD and XRD are different batch.  $T_c$  of the samples were confirmed by magnetization measurements by a superconducting

interference device (SQUID) with an applied field of 10 Oe on MPMS3 (Quantum Design), and the magnetization data are shown in supporting information (Fig. S1). All the examined samples showed bulk superconductivity with a large diamagnetic signal, and the evaluated  $T_c$  for  $\text{CoZr}_2$ ,  $(\text{Fe,Co,Ni})\text{Zr}_2$ , and  $(\text{Fe,Co,Ni,Rh,Ir})\text{Zr}_2$  is 6.0, 3.3, and 5.4 K, respectively.

### 4-3. Statistical Analysis

The obtained XRD and NPD patterns were refined by the Rietveld method using RIETAN-FP,<sup>[35]</sup> and the schematic images of the refined crystal structure were depicted using VESTA.<sup>[36]</sup> In figures of NPD and XRD patterns, we normalize the data by highest intensity to compare the shift in the peaks with changing temperature. The Rietveld refinement results are represented as a mean value with a standard error. The number of data points for linear fitting of lattice constants can be found in the plots in Figs. 2 and 3.

### Supporting Information

Supporting Information is available from the Wiley Online Library or from the author.

### Acknowledgements

The authors would like to thank M. Fujita and O. Miura for their supports in experiments and discussion. This work was performed under the GIMRT Program of the Institute for Materials Research, Tohoku University (CN: Center of Neutron Science for Advanced Materials: Proposal No. 202112-CNKXX-0001). This work was carried out by the JRR-3 program managed by the Institute for Solid State Physics, the University of Tokyo (the T1-3 HERMES IRT program: Proposal No. 22410). This work was partly supported by Grant-in-Aid for Scientific Research (KAKENHI) (Proposal Nos. 21K18834, 21H00151, 19H05164, and 21H00139) and Tokyo Government Advanced Research (H31-1).

### References

- [1] K. Takenaka, *Sci. Technol. Adv. Mater.* (2012) 13, 013001.
- [2] G. D. Barrera, J. A. O. Bruno, T. H. K. Barron, and N. L. Allan, *J. Phys.: Condens. Matter* (2005) 17, R217.
- [3] J. Chen, L. Hu, J. Deng, and X. Xing, *Chem. Soc. Rev.* (2015) 44, 3522.
- [4] T. A. Mary, J. S. O. Evans, T. Vogt, and A. W. Sleight, *Science* (1996) 272, 90.

- [5] K. Takenaka, Y. Okamoto, T. Shinoda, N. Katayama, and Y. Sakai, *Nat. Commun.* (2016) 8, 14102.
- [6] M. Braden, G. André, S. Nakatsuji, and Y. Maeno, *Phys. Rev. B* (1998) 58, 847.
- [7] R. Huang, Y. Liu, W. Fan, J. Tan, F. Xiao, L. Qian, and L. Li, *J. Am. Chem. Soc.* (2013) 135, 11469.
- [8] Y. Y. Zhao, F. X. Hu, L. F. Bao, J. Wang, H. Wu, Q. Z. Huang, R. R. Wu, Y. Liu, F. R. Shen, H. Kuang, M. Zhang, W. L. Zuo, X. Q. Zheng, J. R. Sun, and B. G. Shen, *J. Am. Chem. Soc.* (2015) 137, 1746.
- [9] I. Yamada, K. Tsuchida, K. Ohgushi, N. Hayashi, J. Kim, N. Tsuji, R. Takahashi, M. Matsushita, N. Nishiyama, T. Inoue, T. Irifune, K. Kato, M. Takata, and M. Takano, *Angew. Chem. Int. Ed.* (2011) 50, 6579.
- [10] M. Azuma, W. Chen, H. Seki, M. Czapski, S. Olga, K. Oka, M. Mizumaki, T. Watanuki, N. Ishimatsu, N. Kawamura, S. Ishiwata, M. G. Tucker, Y. Shimakawa, J. P. Attfield, *Nat. Commun.* (2011) 2, 347.
- [11] J. R. Salvador, F. Guo, T. Hogan, M. G. Kanatzidis, *Nature* (2003) 425, 702.
- [12] T. Yokoyama and K. Eguchi, *Phys. Rev. Lett.* (2011) 107, 065901.
- [13] J. Chen, X. R. Xing, G. R. Liu, J. H. Li, and Y. T. Liu, *Appl. Phys. Lett.* (2006) 89, 101914.
- [14] X. R. Xing, J. X. Deng, J. Chen, and G. R. Liu, *Rare Metals* (2003) 22, 294.
- [15] S. L. Bud'ko, N. Ni, S. Nandi, G. M. Schmiedeshoff, and P. C. Canfield, *Phys. Rev. B* (2009) 79, 054525.
- [16] S. A. J. Kimber, D. N. Argyriou, F. Yokaichiya, K. Habicht, S. Gerischer, T. Hansen, T. Chatterji, R. Klingeler, C. Hess, G. Behr, A. Kondrat, and B. Büchner, *Phys. Rev. B* (2008) 78, 140503.
- [17] S. V. Pryanichnikov, S. G. Titova, G. A. Kalyuzhnaya, Yu. I. Gorina, and P. A. Slepukhin, *J. Exp. Theor. Phys.* (2008) 107, 69.
- [18] H. Fujishita, Y. Hayashi, M. Saito, H. Unno, H. Kaneko, H. Okamoto, M. Ohashi, Y. Kobayashi, and M. Sato, *Eur. Phys. J. B* (2012) 85, 52.
- [19] M. S. da Luz, J. J. Neumeier, R. K. Bollinger, A. S. Sefat, M. A. McGuire, R. Jin, B. C. Sales, and D. Mandrus, *Phys. Rev. B* (2009) 79, 214505.
- [20] S. L. Bud'ko, N. Ni, and P. C. Canfield, *Philos. Mag.* (2010) 90, 1219.
- [21] J. J. Neumeier, T. Tomita, M. Debessai, J. S. Schilling, P. W. Barnes, D. G. Hinks, and J. D. Jorgensen, *Phys. Rev. B* (2005) 72, 220505.
- [22] A. F. Clark, G. Fujii, and M. A. Ranney, *IEEE Trans. Magn.* (1981) 17, 2316.

- [23] C. Xin, X. Wang, M. Guan, and Y. Zhou, *J. Supercond. Nov. Magn.* (2015) 28, 437.
- [24] A.V. Pogrebnyakov, J. M. Redwing, S. Raghavan, V. Vaithyanathan, D. G. Schlom, S.Y. Xu, Qi Li, D. A. Tenne, A. Soukiassian, X. X. Xi, M. D. Johannes, D. Kasinathan, W. E. Pickett, J. S. Wu, and J. C. H. Spence, *Phys. Rev. Lett.* (2004) 93, 147006.
- [25] Z. Fisk, R. Viswanathan, and G. W. Webb, *Solid State Commun.* (1974) 15, 1799.
- [26] A. Teruya, M. Kakihana, T. Takeuchi, D. Aoki, F. Honda, A. Nakamura, Y. Haga, K. Matsubayashi, Y. Uwatoko, H. Harima, M. Hedo, T. Nakama, and Y. Ōnuki, *J. Phys. Soc. Jpn.* (2016) 85, 034706.
- [27] Y. Mizuguchi and A. Yamashita, Intechopen (online book chapter), DOI: 10.5772/intechopen.96156.
- [28] Y. Mizuguchi, Md. R. Kasem, and T. D. Matsuda, *Mater. Res. Lett.* (2021) 9, 141.
- [29] Md. R. Kasem, A. Yamashita, Y. Goto, T. D. Matsuda, Y. Mizuguchi, *J. Mater. Sci.* (2021) 56, 9499.
- [30] S. A. J. Kimber, D. N. Argyriou, F. Yokaichiya, K. Habicht, S. Gerischer, T. Hansen, T. Chatterji, R. Klingeler, C. Hess, G. Behr, A. Kondrat, and B. Büchner, *Phys. Rev. B* (2008) 78, 140503.
- [31] T. Tokizono, Y. Tsuru, T. Atsumi, N. Hosokawa, and T. Ohnuma, *J. Cer. Soc. Jpn.* (2016) 124, 744.
- [32] Q. Li, K. Lin, Z. Liu, L. Hu, Y. Cao, J. Chen, and X. Xing, *Chem. Rev.* (2022) 122, 8438.
- [33] K. Ohoyama, T. Kanouchi, K. Nemoto, M. Ohashi, T. Kajitani, and Y. Yamaguchi, *Jpn. J. App. Phys.* (1998) 37, 3319.
- [34] Y. Nambu et al., under preparation.
- [35] F. Izumi and K. Momma, *Solid State Phenom.* (2007) 130, 15.
- [36] K. Momma and F. Izumi, *J. Appl. Crystallogr.* (2011) 44, 1272.

## Supporting Information

### Anomalous thermal expansion in a CuAl<sub>2</sub>-type superconductor CoZr<sub>2</sub>

Yoshikazu Mizuguchi<sup>1\*</sup>, Md. Riad Kasem<sup>1</sup>, Yoichi Ikeda<sup>2</sup>

<sup>1</sup>Department of Physics, Tokyo Metropolitan University, Hachioji, Tokyo 192-0397, Japan.

<sup>2</sup>Institute for Materials Research, Tohoku University, Sendai, Miyagi 987-6543, Japan

E-mail: mizugu@tmu.ac.jp

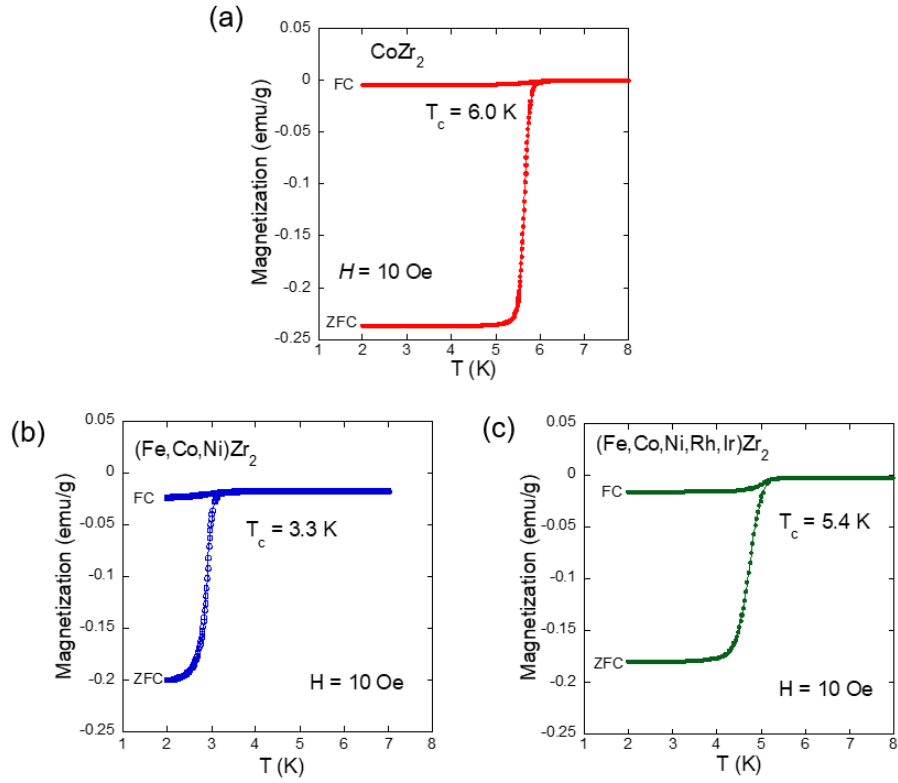


Fig. S1. Temperature dependence of magnetization after zero-field cooling (ZFC) and field cooling (FC) for  $TrZr_2$  samples used in this study.

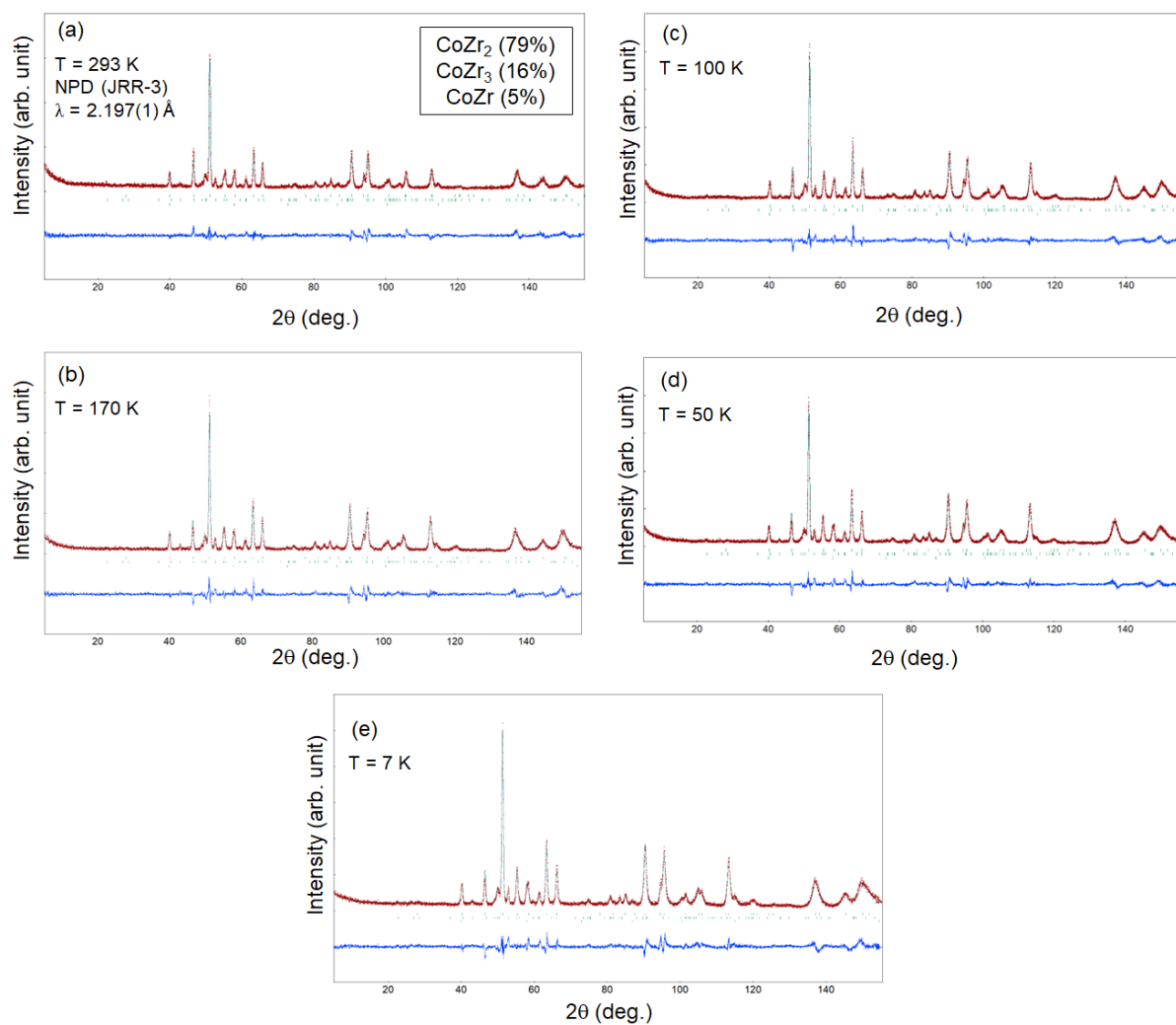


Fig. S2. Rietveld refinement results for NPD data for  $\text{CoZr}_2$  collected at (a) 293 K, (b) 170 K, (c) 100 K, and (d) 50 K.

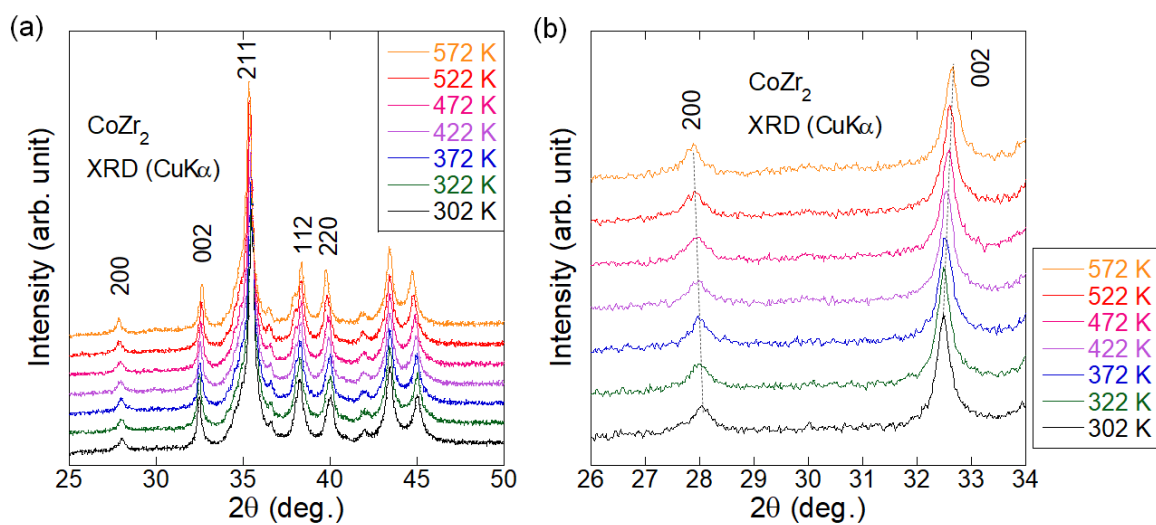


Fig. S3. (a) High-temperature powder XRD patterns for  $\text{CoZr}_2$ . (b) XRD profiles near 200 and 002 peaks. The numbers indicate Miller indices.

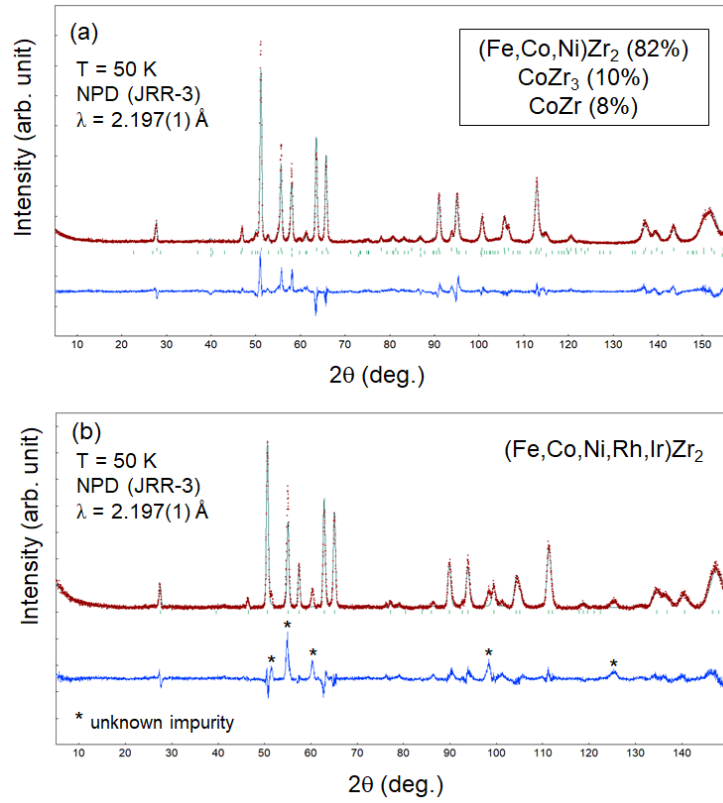


Fig. S4. Rietveld refinement results for NPD data collected at 50 K on (a)  $\text{Fe}_{1/3}\text{Co}_{1/3}\text{Ni}_{1/3}\text{Zr}_2$  and (b)  $\text{Fe}_{0.2}\text{Co}_{0.2}\text{Ni}_{0.2}\text{Rh}_{0.2}\text{Ir}_{0.2}\text{Zr}_2$ . For  $\text{Fe}_{1/3}\text{Co}_{1/3}\text{Ni}_{1/3}\text{Zr}_2$ , three-phase refinement was performed, and single-phase refinement was applied for  $\text{Fe}_{0.2}\text{Co}_{0.2}\text{Ni}_{0.2}\text{Rh}_{0.2}\text{Ir}_{0.2}\text{Zr}_2$ .

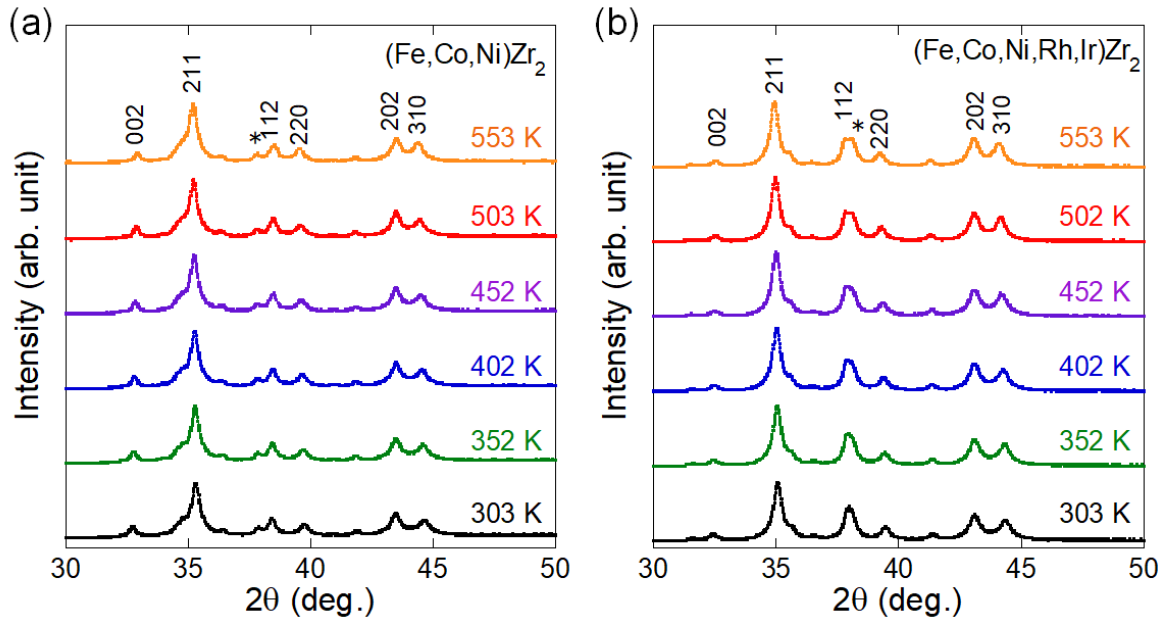


Fig. S5. (a) High-temperature powder XRD patterns for  $(\text{Fe,Co,Ni})\text{Zr}_2$ . (b) High-temperature powder XRD patterns for  $(\text{Fe,Co,Ni,Rh,Ir})\text{Zr}_2$ . The numbers indicate Miller indices. Asterisks indicate impurity phases.



**Table S1.** Structural parameters of (Fe,Co,Ni)Zr<sub>2</sub> obtained from the Rietveld refinement. The atomic coordinates for the Zr and Tr site are (x, x+0.5, 0) and (0, 0, 0.25), respectively.

	$T = 293$ K	$T = 250$ K	$T = 170$ K	$T = 100$ K	$T = 50$ K	$T = 7$ K
$a$ (Å)	6.3953(2)	6.3881(2)	6.3775(2)	6.3694(2)	6.3653(2)	6.3644(2)
$c$ (Å)	5.4438(2)	5.4505(2)	5.4580(2)	5.4651(2)	5.4702(2)	5.4719(2)
$V$ (Å <sup>3</sup> )	222.655(14)	222.423(12)	221.994(11)	221.713(12)	221.639(12)	221.640(12)
$R_{wp}$ (%)	20.7	18.1	16.1	15.9	16.3	15.8
$S$	2.2	2.3	2.0	2.1	2.1	2.4
$x$ (Zr)	0.1693(3)	0.1690(2)	0.1685(2)	0.1692(2)	0.1701(2)	0.1697(2)
$U_{iso}$ for Zr (Å <sup>2</sup> )	0.0342(9)	0.0211(8)	0.0174(7)	0.0167(7)	0.0178(7)	0.0175(7)
Tr-Zr (Å)	2.738(2)	2.7374(12)	2.7361(12)	2.7327(12)	2.7299(12)	2.7307(12)
Tr-Tr (i) (Å)	2.72190(11)	2.72525(11)	2.72900(11)	2.73255(11)	2.73510(11)	2.73595(10)
Tr-Tr (ii) (Å)	4.5222(2)	4.5171(2)	4.5096(2)	4.5039(2)	4.5010(2)	4.50031(10)
Zr-Zr (i) (Å)	3.089(2)	3.0934(13)	3.0998(13)	3.0961(13)	3.0903(12)	3.0943(9)
Zr-Zr (ii) (Å)	3.360(3)	3.358(2)	3.354(2)	3.347(2)	3.341(2)	3.342(2)
Zr-Tr-Zr angle (deg.)	120.39(4)	120.29(3)	120.17(3)	120.00(3)	119.87(3)	119.87(4)

**Table S2.** Structural parameters of (Fe,Co,Ni,Rh,Ir)Zr<sub>2</sub> obtained from the Rietveld refinement. The atomic coordinates for the Zr and Tr site are (x, x+0.5, 0) and (0, 0, 0.25), respectively.

	$T = 293$ K	$T = 250$ K	$T = 100$ K	$T = 50$ K	$T = 7$ K
$a$ (Å)	6.4400(3)	6.4326(3)	6.4252(3)	6.4218(3)	6.4200(3)
$c$ (Å)	5.4987(4)	5.5154(3)	5.5190(3)	5.5239(3)	5.5239(3)
$V$ (Å <sup>3</sup> )	228.05(2)	228.22(2)	227.83(2)	227.80(2)	227.68(2)
$R_{wp}$ (%)	23.5	22.6	20.6	21.4	20.3
$S$	1.7	2.0	1.9	2.0	2.1
$x$ (Zr)	0.1673(3)	0.1694(3)	0.1693(2)	0.1687(2)	0.1684(2)
$U_{iso}$ for Zr (Å <sup>2</sup> )	0.0277(12)	0.0188(10)	0.0185(9)	0.0193(9)	0.0166(9)
Tr-Zr (Å)	2.764(2)	2.759(2)	2.7571(12)	2.7581(12)	2.7583(12)
Tr-Tr (i) (Å)	2.7494(3)	2.7577(2)	2.7595(2)	2.7620(2)	2.7612(2)
Tr-Tr (ii) (Å)	4.5537(3)	4.5485(3)	4.5433(3)	4.5409(3)	4.5396(2)
Zr-Zr (i) (Å)	3.135(2)	3.123(2)	3.1250(13)	3.1319(13)	3.1343(9)
Zr-Zr (ii) (Å)	3.392(3)	3.379(3)	3.376(2)	3.376(2)	3.377(2)
Zr-Tr-Zr angle (deg.)	120.36(5)	120.03(5)	119.94(3)	119.91(3)	119.91(4)